Zoledronic Acid Inhibits Both the Osteolytic and Osteoblastic Components of Osteosarcoma Lesions in a Mouse Model

Agatha Labrinidis,[1] Shelley Hay,[1] Vasilios Liapis,[1] Vladimir Ponomarev,[2] David M. Findlay,[1] and Andreas Evdokiou[1]

Abstract

Purpose: To evaluate the efficacy of zoledronic acid (ZOL) against osteosarcoma (OS) growth, progression, and metastatic spread using an animal model of human OS that closely resembles the human disease.

Experimental Design: Human K-HOS or KRIB OS cells, tagged or untagged with a luciferase reporter construct, were transplanted directly into the tibial cavity of nude mice. ZOL was given as weekly, or a single dose of 100 μg/kg body weight, equivalent to the 4 mg i.v. dose used clinically. Tumor growth at the primary site and as pulmonary metastases was monitored by bioluminescence imaging and histology, and OS-induced bone destruction was measured using high-resolution micro–computed tomography.

Results: Mice transplanted with OS cells exhibited aberrant bone remodeling in the area of cancer cell transplantation, with areas of osteolysis mixed with extensive new bone formation extending from the cortex. ZOL administration prevented osteolysis and significantly reduced the amount of OS-induced bone formation. However, ZOL had no effect on tumor burden at the primary site. Importantly, ZOL failed to reduce lung metastasis and in some cases was associated with larger and more numerous metastatic lesions.

Conclusions: Our data show that clinically relevant doses of ZOL, while protecting the bone from OS-induced bone destruction, do not inhibit primary tumor growth. Moreover, lung metastases were not reduced and may even have been promoted by this treatment, indicating that caution is required when the clinical application of the bisphosphonate class of antiresorptives is considered in OS.

Osteogenic sarcoma, commonly referred to as osteosarcoma (OS), is the most frequent primary malignancy of the skeleton, developing mainly before the age of 30 years (1, 2). Metastatic spread, preferentially to the lungs, is seen in 20% of presenting patients and is correlated with poor survival statistics (3–5). Bone lesions caused by OS are characterized based on their radiologic appearance and appear as either osteolytic, osteoblastic (osteosclerotic), or mixed (6). Osteolysis is a common manifestation associated with OS, even within predominantly osteoblastic lesions, and is mediated primarily by osteoclasts and their bone-resorbing activity (7, 8). Factors released from the bone are believed to stimulate tumor growth and tumor cells are in turn able to produce factors that stimulate osteoclast differentiation and activity. This results in the establishment of a host-tumor relationship, often termed "the vicious cycle" due to its progressively destructive nature (9). By mechanisms that are not well understood, tumor cells associated with osteoblastic lesions can stimulate osteogenesis (10, 11).

Bisphosphonates (BP) are commonly used for the prevention and treatment of various bone diseases associated with enhanced bone resorption, such as Paget's disease and osteoporosis (12, 13). In addition to their antiresorptive activity, there is growing evidence supporting the direct effects of BPs on cancer cells themselves, at least *in vitro*. In this respect, zoledronic acid (ZOL) exhibits the highest potency of its class. The antitumor activity of BPs has been shown in a wide variety of tumor cell types, including leukemia (14), breast cancer (15), prostate cancer (16), and OS (17, 18). These *in vitro* studies have shown that BPs can dose dependently inhibit proliferation and induce apoptosis in tumor cells. A reduction by BPs in tumor cell adhesion, invasion, and angiogenesis has also been reported, making BPs potentially attractive agents in the treatment of metastatic cancers (19).

Preclinical animal models of metastatic cancer have shown a reduction in tumor-induced osteolysis with ZOL treatment (20–22). Reports of animal models of prostate cancer have all shown reduced osteolysis with ZOL treatment, with conflicting

Authors' Affiliations: [1]Discipline of Orthopaedics and Trauma, University of Adelaide, The Royal Adelaide Hospital and The Hanson Institute, Adelaide, South Australia, Australia and [2]Department of Neurology, Memorial Sloan-Kettering Cancer Center, New York, New York

Received 6/24/08; revised 1/9/09; accepted 2/19/09; published OnlineFirst 4/28/09.

Grant support: Cancer Council of South Australia and Australian Orthopaedics Association.

The costs of publication of this article were defrayed in part by the payment of page charges. This article must therefore be hereby marked *advertisement* in accordance with 18 U.S.C. Section 1734 solely to indicate this fact.

Requests for reprints: Andreas Evdokiou, Discipline of Orthopaedics and Trauma, Level 4, Bice Building, Royal Adelaide Hospital, North Terrace, Adelaide 5000, South Australia, Australia. Phone: 61-8-8222-3107; Fax: 61-8-8232-3065; E-mail: andreas.evdokiou@adelaide.edu.au.

doi:10.1158/1078-0432.CCR-08-1616

Translational Relevance

Osteosarcoma (OS) is the most common primary malignant tumor of bone in children and adolescents. Despite significant improvements in treatment of the primary tumor, a significant proportion of OS patients eventually develop lung metastases and succumb to their disease even after multistage conventional chemotherapy and surgical excision. Therefore, there is a need to develop new and safe approaches to the treatment of OS. There is now extensive evidence that bisphosphonates (BP), and in particular the newer nitrogen-containing BPs including zoledronic acid (ZOL), have antitumor activity and can reduce skeletal and perhaps also extraskeletal tumor burden in a variety of tumor types. This study has shown that ZOL is able to inhibit the development and progression of not only the osteolytic but also the osteoblastic component of primary OS lesions in an animal model that closely resembles the human disease. Surprisingly, however, we found that in spite of the protective effects of ZOL on OS-induced bone destruction, treatment with clinically compatible doses of ZOL did not reduce and may have even promoted lung metastases. Because BP treatment is of growing interest in OS therapy, our findings may have important clinical implications when considering the treatment of patients with OS with this class of drug.

results in osteoblastic lesions (23). Clinically, BP treatment is the current standard of care for palliative treatment of bone metastases (24). ZOL has proven to be effective in large nonrandomized clinical trials and is the first BP to show significant clinical benefit in patients with bone metastases from various primary tumors (19). Prolonged treatment with ZOL seems to be safe and well tolerated, and this combination of potency and safety makes it a useful adjuvant therapy in bone metastasis (25).

We report here that although ZOL treatment had a significant protective effect on OS-induced bone destruction, it did not inhibit primary tumor growth or reduce lung metastases and in some cases even promoted lung metastases in a xenograft mouse model that closely mimics the clinical outcome of patients with OS.

Materials and Methods

Cells and reagents. The human OS cell line K-HOS was obtained from the American Type Culture Collection. The KRIB (26) cell line was kindly provided by Dr. Berlin (Sahlgren University Hospital, Gothenburg, Sweden). Cells were cultured in DMEM supplemented with glutamine (2 mmol/L), penicillin (100 IU/mL), streptomycin (100 μg/mL), gentamicin (160 μg/mL), and 10% fetal bovine serum (Biosciences) in a humidified atmosphere containing 5% CO_2.

ZOL was generously provided by Novartis Pharma AG. The tetrapeptide caspase inhibitor zVAD-fmk was purchased from Calbiochem and geranylgeraniol (GGO) was purchased from MP Biomedicals.

Measurement of cell viability and apoptosis analysis. Cells (1×10^4) were incubated for 72 h with increasing concentrations of ZOL (0.1-100 μmol/L). Cell viability was determined by staining with crystal violet and measuring absorbance at 570 nm wavelength. The experiments were done in quadruplicate and repeated at least thrice. Results of representative experiments are given as the mean ± SD. Apoptosis analysis, including 4′,6-diamidino-2-phenylindole (DAPI) staining, caspase activation, and caspase inhibition, was done as described previously (17).

Retroviral infection of K-HOS cells with the triple reporter gene construct SFG-NES-TGL. Luciferase-expressing K-HOS cells were generated using the retroviral expression vector SFG-NES-TGL (27). Virus particle–containing supernatants were generated and filtered to remove any cellular debris and then used to infect K-HOS cells, as described previously (28). The retrovirally transduced K-HOS cells were grown as bulk cultures for 48 h and subsequently sorted for positive green fluorescent protein (GFP) expression using fluorescence-activated sorting (FACS; Aria, BD Biosciences). The cells were allowed to proliferate and the 10% of cells expressing GFP most strongly were obtained by FACS to generate the subline K-HOS-NES-TGL.

Mouse model of OS. Four-week-old female BALB/c *nu/nu* mice were housed under pathogen-free conditions in accordance with the guidelines approved by the Institute of Medical and Veterinary Science animal ethics research committee. The left tibia was wiped with 70% ethanol and a 27-gauge needle coupled to a Hamilton syringe was inserted through the tibial plateau with the knee flexed, and 1×10^5 K-HOS-NES-TG cells, resuspended in 10 μL PBS, were injected into the marrow space of the proximal tibia. As a control, all animals were injected with PBS in the contralateral tibia. Mice were randomly assigned into three groups of 10 animals each, and starting 1 wk after cancer cell implantation, 100 μg/kg body weight ZOL was given as weekly, or as a single dose, equivalent to the 4 mg i.v. dose given to patients. Similarly, untagged parental KRIB cells were injected intratibially, and mice were randomly assigned into vehicle ($n = 6$) or the ZOL (once only; $n = 6$) treatment groups.

In vivo *bioluminescence imaging*. Noninvasive, whole-body imaging to monitor luciferase-expressing K-HOS-NES-SFG-TGL cells in mice was done weekly using the IVIS 100 Imaging system (Xenogen). Mice were injected i.p. with 100 μL of the D-luciferin solution at 250 mg/kg body weight (Xenogen) and then gas anaesthetized with isoflurane (Faulding Pharmaceuticals). Images were acquired for 0.5 to 10 s and the photon emission transmitted from mice was captured and quantitated in photons/second using Xenogen Living Image (Igor Pro version 2.5) software.

Micro–computed tomography analysis. Both the right and left tibiae of each animal were mounted in the CT specimen tube and placed securely into the SkyScan-1072 X-ray micro–computed tomography (μCT) scanner. Scanning was commenced with magnification set to give scan slices of 17.8 or 5.2 μm, respectively. Three-dimensional images were generated using Cone-Beam reconstruction and three-dimensional visualization (SkyScan). Using the two dimensional images obtained from the μCT scan, the growth plate was identified and 750 sections, starting from the growth plate/tibial interface and moving down the tibia, were selected. Bone volume (mm^3) was generated and compared with the control tibia for each animal.

Histology. Tibiae were fixed in 10% buffered formalin followed by acid decalcification in 10% EDTA solution and 7% nitric acid at room temperature. Samples were paraffin embedded, sectioned longitudinally at 6 μm, and stained with H&E. Analysis was done on a Nikon Eclipse TE300 inverted microscope (Nikon Corp.). Tumor size, defined as the tumor area, was calculated from the section of the tibia that best represents the center of the tumor mass and expressed as an average tumor area per group in absolute units (mm^2).

Statistical analysis. The continuous outcome bone volume was analyzed using mixed-model ANOVA to allow for clustering of mice (i.e., more than one observation per mouse). Post hoc pairwise comparisons were undertaken with no adjustment made for multiple comparisons.

Results

Effect of ZOL on cell proliferation and apoptosis of K-HOS cells. The effect of ZOL on cell proliferation and apoptosis was tested in the K-HOS human OS cell line. Treatment with

ZOL for 72 hours resulted in a dose-related inhibition of cellular proliferation of K-HOS cells in monolayer cultures (Fig. 1A). Exposure to concentrations of ZOL >10 μmol/L resulted in marked cytotoxicity, with cells detaching from the substratum and cell death occurring within 48 to 72 hours. Morphologic evidence of apoptosis, including chromatin condensation, nuclear fragmentation, and the formation of dense rounded apoptotic bodies, was seen at doses greater than the half-maximal effective dose of 15 μmol/L (data not shown). ZOL-induced apoptotic cell death was concomitant with a dose-related increase in caspase-3–like activity (Fig. 1B). To investigate the role of caspase activation in the ZOL-mediated apoptosis of K-HOS cells, the effect of caspase inhibition on the induction of apoptosis was examined. Cells were incubated for 72 hours with 15 μmol/L ZOL either alone or in the presence of the broad specificity caspase inhibitor zVAD-fmk. Consistent with our previously published data in other OS cell lines (17), the inhibition of caspase activity failed to protect K-HOS cells from ZOL-induced cell death, suggesting that ZOL-induced apoptosis of K-HOS cells is independent of caspase activation (Fig. 1C). To examine the involvement of the mevalonate pathway on the ZOL-mediated apoptosis of K-HOS cells, we assessed the ability of GGO, an intermediate of the mevalonate pathway, to protect cells from ZOL-induced apoptosis. The addition of 300 μmol/L GGO significantly protected K-HOS cells from ZOL-induced apoptosis, whereas GGO alone had no effect on cell number (Fig. 1C). Lysates from control untreated cells, and cells treated with 30 μmol/L ZOL, were collected after 48 hours and analyzed by Western blotting for the presence of prenylated and the nonprenylated forms of the small GTPase, Rap1A. Untreated cells expressed only the prenylated

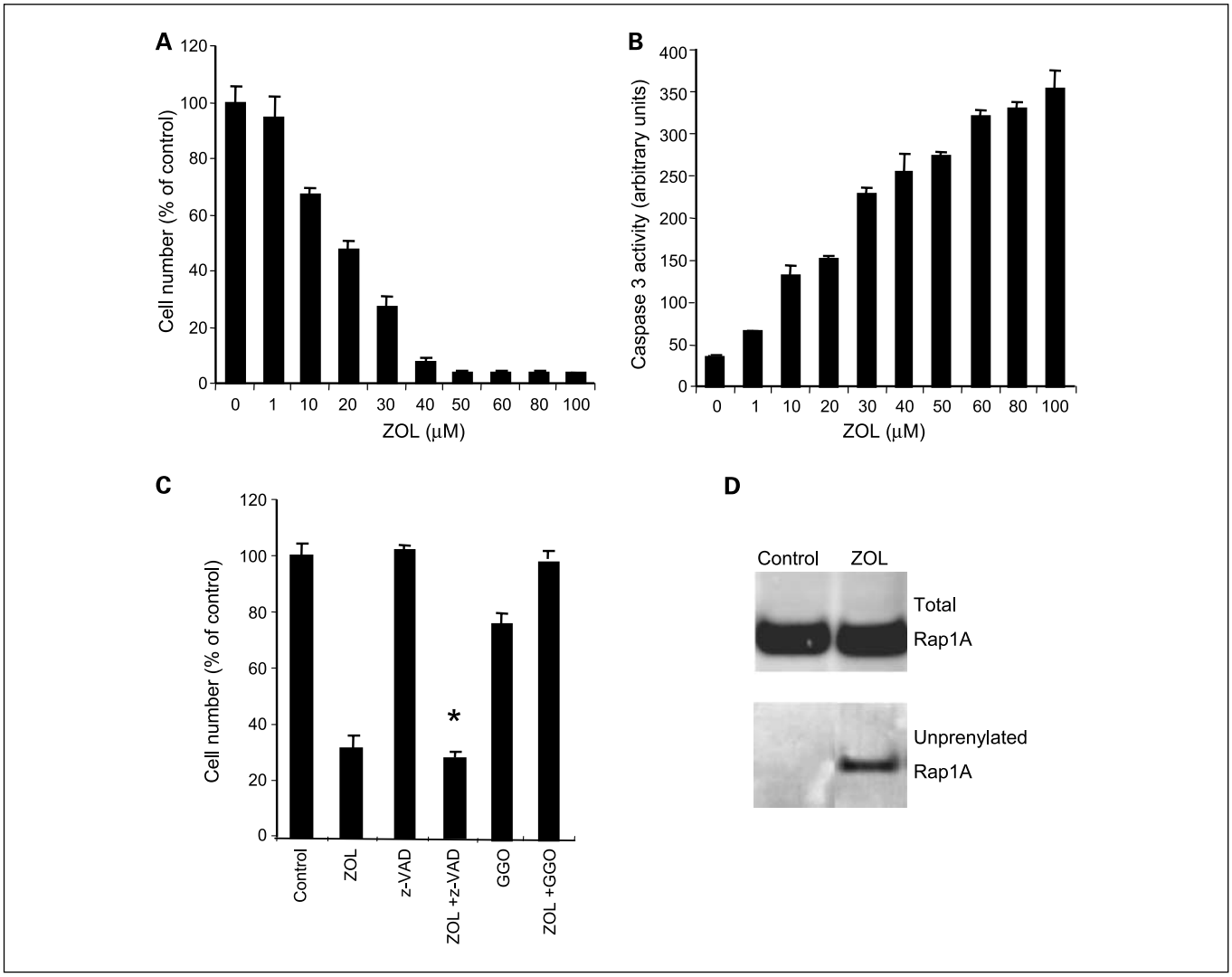

Fig. 1. ZOL-mediated induction of apoptosis in K-HOS OS cells *in vitro*. *A,* K-HOS cells were incubated for 72 h in medium containing increasing concentrations of ZOL (0-100 μmol/L) and cell number as a percentage of control untreated cells was determined. *B,* cell lysates were used to determine caspase-3–like activity using the caspase-3–specific fluorogenic substrate, zDEVD-AFC, as described previously (17). The data show a dose-dependent increase in caspase-3 activity. *C,* the effect of the broad specificity caspase inhibitor zVAD-fmk on cell survival was assessed, both alone and in combination with ZOL (*, $P < 0.00001$), and cell number was determined. Similarly, the effect of GGO, an intermediate of the mevalonate pathway, was assessed in cells treated with and without ZOL. Columns, mean of triplicate results from a representative experiment, repeated at least twice; bars, SD. *D,* Western blot analysis revealed the presence of unprenylated Rap1A protein in lysates of cells treated with ZOL but not in the control cells.

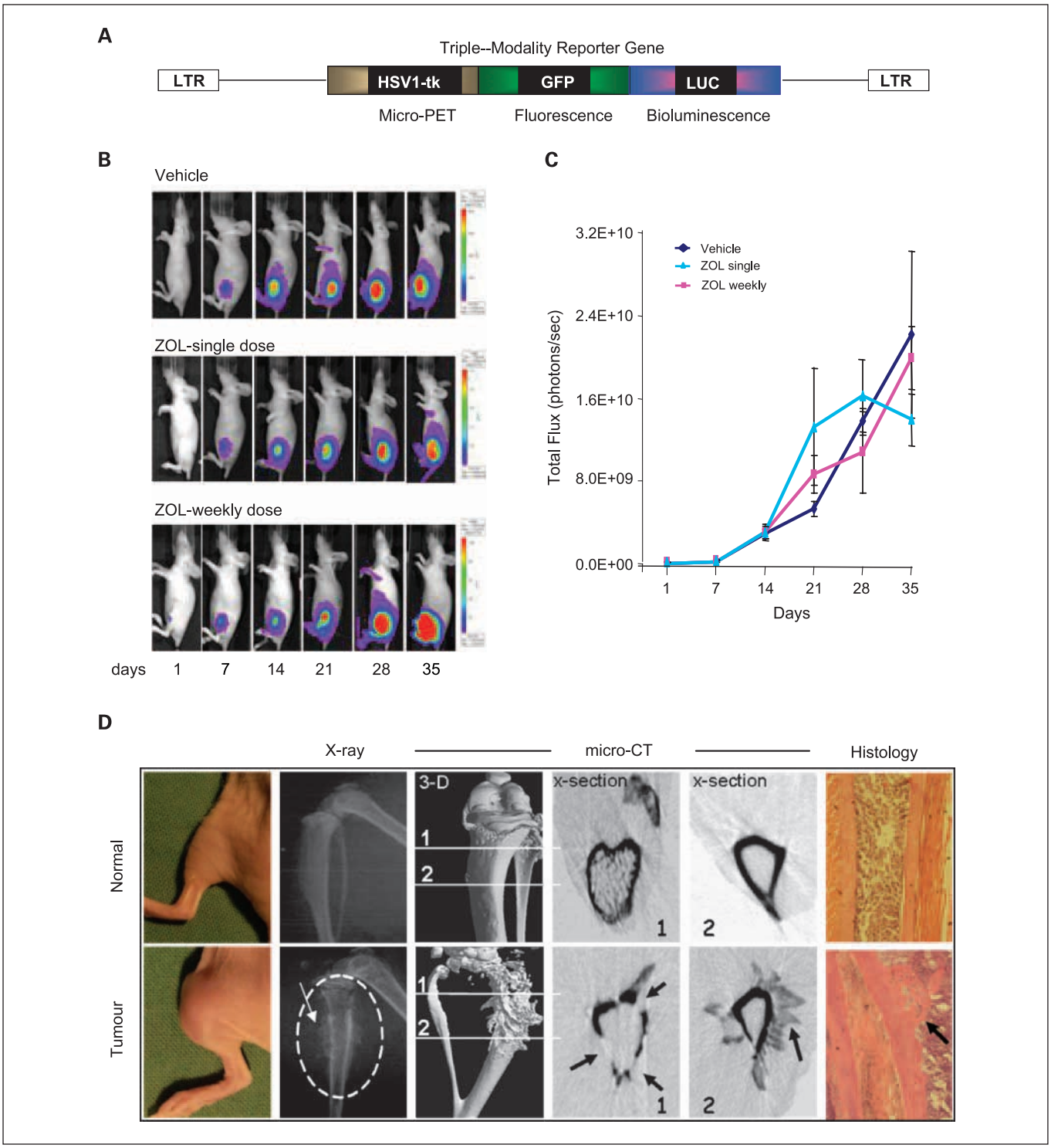

Fig. 2. Effect of ZOL treatment on tumor growth, assessed by noninvasive *in vivo* BLI, and OS-induced bone destruction. *A,* triple reporter retroviral gene construct NES-TGL was used to infect K-HOS OS cells. After infection, K-HOS cells were FACS sorted for high level expression of GFP and analyzed for luciferase activity *in vitro. B,* nude mice were injected with 1×10^5 K-HOS-NES-TGL cells into the left tibia, whereas the right contralateral tibia was injected with PBS alone as an internal control. Mice were randomized into three groups of 10 mice per group. One week after cancer cell transplantation, ZOL was administered (s.c.), either as a single dose of 100 μg/kg/dose or as a once weekly dose (100 μg/kg/dose), until termination of the experiment. The vehicle-treated animals received s.c. injections of PBS, adhering to the same schedule as ZOL administration. Mice were imaged weekly using the Xenogen IVIS 100 BLI system. Representative whole-body images of one animal per group are shown over the course of the experiment. *C,* BLI measurements are expressed as the sum of integrated photon counts per second. Points, mean; bars, SE. *, $P < 0.01$. *D,* tumor at 5 wk after cancer cell transplantation breaks through the bone cortex and extends into the surrounding soft tissue. Radiographs showing areas of osteolysis and areas of new bone formation extending from the periosteum and cortex are shown (*arrow*). Shown also are *ex vivo* three-dimensional reconstructed μCT images and serial cross-sectional views with progressive loss of trabecular and cortical bone from representative tibiae (*arrows*). Also shown is an extensive network of mineralized new bone extending perpendicular from the periosteum and cortex. Histologic sections showing that new bone formation is mineralized woven bone and in contact with the cortex.

form of Rap1A, whereas in the ZOL-treated cells both prenylated and unprenylated Rap1A were present (Fig. 1D). These results are consistent with the importance of the mevalonate pathway as an intracellular target for the effects of ZOL.

Effect of ZOL on the development, progression, and metastatic spread of human OS in a mouse model. A limitation in measuring tumor burden in bone is that it is not possible to accurately assess the progression of tumor growth by palpation, as in soft tissue tumors, before they break through the cortical bone. To overcome this limitation, we used noninvasive bioluminescence imaging (BLI), which enabled sensitive real-time *in vivo* tracking of OS growth in bone and its metastatic spread. The parental K-HOS human OS cells (29) were retrovirally infected with a triple-fusion protein reporter construct encoding herpes simplex virus thymidine kinase, GFP, and firefly luciferase. After infection, K-HOS cells were enriched for high-level expression of GFP by two rounds of fluorescence-activated cell sorting, thus generating the subline K-HOS-NES-TGL (Fig. 2A). The selected cells exhibited a 1,000-fold induction of luciferase activity when analyzed *in vitro*. When compared with the parental noninfected cells, K-HOS-TGL cells were equally responsive to ZOL treatment on both cell survival and kinetics of caspase activation (data not shown).

When injected into bone, these tumor cells produce mixed osteolytic/osteoblastic lesions directly in the area of injection. As in the human disease, K-HOS cells from the intraosseous tumors reproducibly form pulmonary metastases that are easily quantifiable with BLI, and by histologic inspection of the lungs, 5 to 6 weeks after cancer cell inoculation. K-HOS-NES-TGL cells were injected intratibially in 4- to 6-week-old BALB/c *nu/nu* female mice. Thirty animals were inoculated and animals were then assigned randomly into three groups: (*a*) the control untreated group, (*b*) the ZOL weekly treated group, and (*c*) the ZOL single dose. To allow establishment of tumor cells within the bone environment, ZOL treatment was commenced 7 days after cancer cell transplantation and ZOL was then administered s.c. at a dose of 100 μg/kg either once weekly until sacrifice or as a single dose. Results showed an exponential increase of photon emission associated with an increase in tumor burden, which was clearly evident from day 7 onwards in both the weekly and single dosing regimens (Fig. 2B). This trend was not significantly different from that of the vehicle-treated animals, indicating that ZOL treatment has no measurable effect on tumor burden at the primary site (Fig. 2C).

X-ray images of tumor-bearing tibiae taken just before sacrifice confirmed the presence of osteolysis in all animals within the control vehicle group. A characteristic radiodense "sunburst" configuration, consistent with spicular new bone formation, was also evident, extending perpendicularly to the periosteum and into the surrounding soft tissues (Fig. 2D). In contrast to radiography, which only provides two-dimensional images, μCT offers the advantage of generating three-dimensional images that can be quantified. Reconstructed three-dimensional images of μCT scans showed extensive bone remodeling, characterized by large osteolytic and osteoblastic activity in the tumor-bearing tibiae (Fig. 2D). Cross-sections of the μCT images of the normal non–tumor-bearing tibiae revealed a smooth surface of the cortical bone with an intact endocortical trabecular network. In contrast, significant cortical bone destruction and loss of trabecular architecture were apparent in all tumor-bearing tibiae, representing the osteolytic component of OS lesions. In addition, marked spicular new bone formation, extending from the periosteum, was clearly evident in all tumor-bearing tibiae, confirming the radiographic data (Fig. 2D). Histologic analysis showed that the spicular new bone was mineralized woven bone and was not in the tumor mass but was an extension of, and in contact with, the periosteum and cortex (Fig. 2D).

In animals treated with either the single or weekly dosing regimen of ZOL, qualitative assessment of bone architecture showed remarkable conservation of the tibiae, with no radiographic or μCT evidence of cortical or trabecular bone destruction (Fig. 3A). In addition, the periosteal new bone formation was significantly reduced by the single dose of ZOL and was almost absent in animals receiving the weekly dose regimen (Fig. 3A). Closer examination of the radiographic images showed that in all of the ZOL-treated animals, from both treatment regimens, but not in the vehicle-treated animals, the bones were highly radiodense, reflecting increases in mineral content, likely due, in these young growing animals, to ongoing bone formation and inhibition of bone resorption. This effect of ZOL and other BPs was striking in the distal femurs and proximal tibiae and was not restricted to the tumor site, being also observed in the contralateral non–tumor-bearing tibiae, as reported in several other studies (Fig. 3A and B; refs. 30–35).

In addition to the qualitative assessment of bone architecture, morphometric parameters were quantified from the three-dimensional μCT data generated after termination of the K-HOS experiments using the high-resolution desktop μCT. We compared the left tumor-bearing tibiae with the contralateral right non–tumor-bearing tibiae at a selected region, beginning at the growth plate and extending downwards 750 × 5 μm slices. This region encompassed all of the OS lesions. In the untreated animals, there was a mean net increase of 36% in the total bone volume in the left tumor-bearing tibiae in comparison with the contralateral right non–tumor-bearing tibiae of the same animals ($L = 3.5 \pm 0.4$ mm^3 versus $R = 2.6 \pm 0.48$ mm^3), which was a composite of osteolytic and osteoblastic activity by the tumors (Fig. 3C). With ZOL treatment, the total bone volume increased significantly in both the tumor-bearing and non–tumor-bearing tibiae when compared with vehicle (Fig. 3C). However, the percentage increase in bone volume induced by the tumors was significantly reduced in both the single and weekly ZOL dosing regimen, compared with the untreated control, suggesting that inhibition of osteoclastic activity by ZOL leads also to inhibition of tumor-induced osteoblastic activity (Fig. 3D). The effect of ZOL on trabecular bone parameters was also quantified from the μCT data. Table 1 shows that the derived histomorphometric parameters were consistent with the increased bone seen with ZOL, with increased trabecular number and bone surface and decreased trabecular space. Trabecular thickness was not affected by ZOL treatment. The effects of ZOL on trabecular structure were found in both the tumor-bearing tibiae and the contralateral non–tumor-bearing tibiae (Table 1).

At the end of the experiment, the lungs from each group of animals were excised and tumor burden, as a function of photon counts per second, was quantified *ex vivo* using BLI (Fig. 4A). The mean luciferase activity of lungs from mice treated with both the weekly and single dosing regimen of ZOL was significantly higher than that of the vehicle-treated animals (Fig. 4B). These

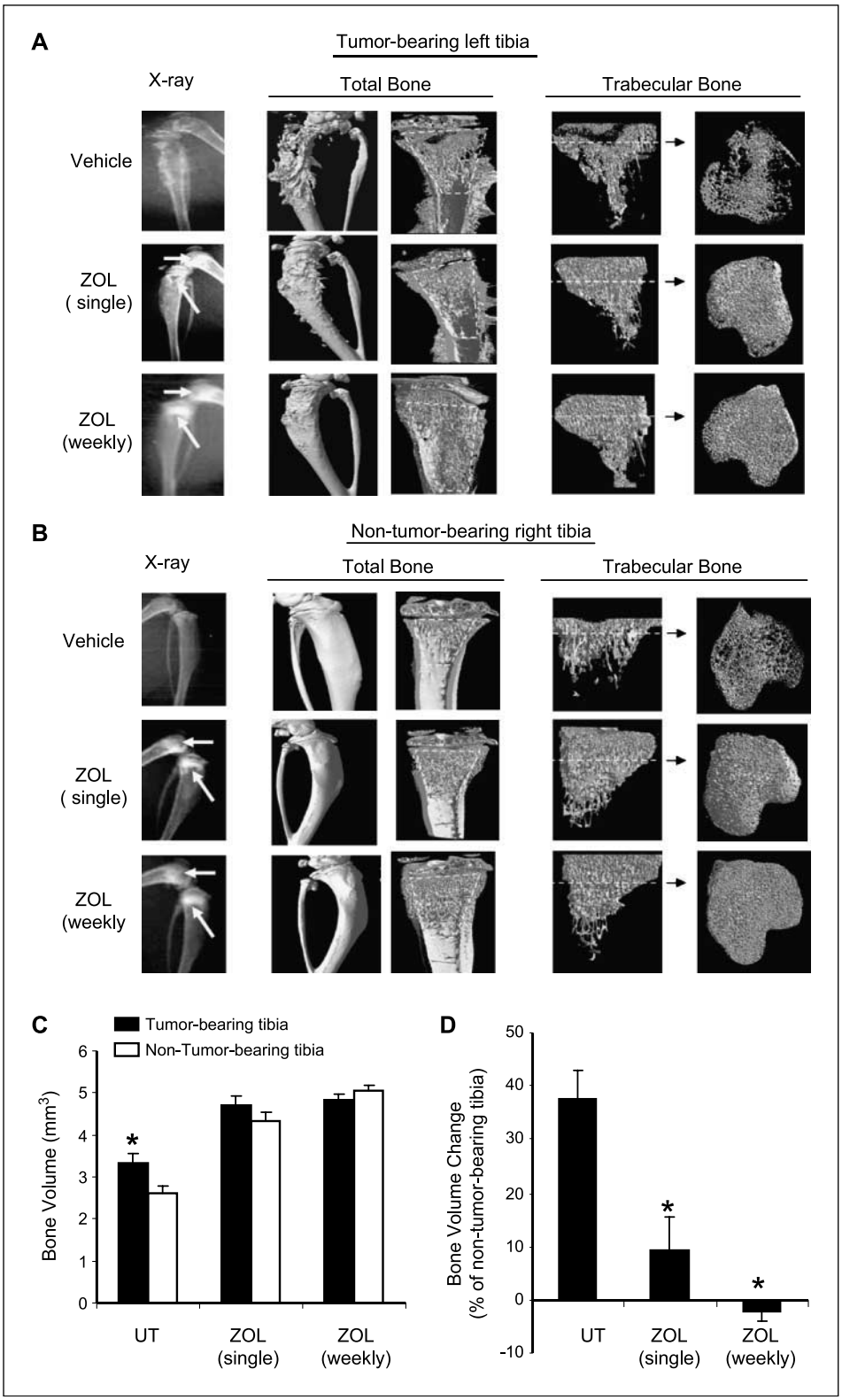

Fig. 3. Qualitative and quantitative assessment of bone architecture with ZOL treatment. Radiographic and *ex vivo* μCT images of tumor-bearing (*A*) and contralateral non–tumor-bearing (*B*) tibiae from ZOL-treated and vehicle-treated mice. Transverse and cross-section views of representative tibiae show loss of cortical and trabecular bone in tumor-bearing tibia with new bone extending from the cortex. ZOL treatment given once only or weekly inhibited OS-induced bone destruction and increased trabecular density in both tumor and non–tumor-bearing tibiae. ZOL treatment increased radiodensity in areas of increased bone turnover, at the proximal tibia and distal femur, in both tumor and non–tumor-bearing tibiae. All images were obtained at termination of the experiment on day 35 after cancer cell transplantation. The images shown are examples that best illustrate the effects of the treatments. Arrows, increased radiodensity. *C,* bone volume comparisons between the control untreated (*UT*) group and the single and weekly ZOL-treated groups. The chart shows the average total bone volume in each group for both the tumor-bearing (■) and non–tumor-bearing tibiae (□). *, $P < 0.05$, with respect to the non–tumor-bearing control. *D,* right, percentage change of bone in the tumor-bearing tibiae of each group compared with the contralateral tibiae. *, $P < 0.05$, with respect to the untreated control. Bone volume was measured from 750 μCT sections of the proximal tibia, starting from the growth plate and using the program CTan. Data shown in each case are the average bone volume from all animals in that group. Columns, mean; bars, SE.

results indicate that, in addition to ZOL having no effect on OS burden within bone, it actually increased the propensity of K-HOS cells to metastasize to lungs.

To substantiate these observations, we did a second independent experiment using parental untagged K-HOS cells. Twenty animals were inoculated and animals were then assigned randomly into two groups: (*a*) the control untreated group and (*b*) the ZOL weekly treated group. The rate at which the parental K-HOS cells established tumors in the tibia was 85% of injected animals (8 in the untreated control group and 9 in

the ZOL-treated group). In the absence of BLI, successful implantation was manifested by visible tumors in all animals by 3 weeks after cancer cell transplantation, as tumors penetrated the cortex and extended into the surrounding soft tissue. Tumor burden at the primary site and metastatic spread to the lungs were assessed histologically. Tumor area was calculated from histologic sections of the tibia that best represented the center of the tumor mass and was expressed as an average tumor area per group in absolute units (mm^2). Tumor volume was also measured from μCT analysis software, as described in Materials and Methods. As with the first experiment, ZOL treatment had no effect on tumor burden at the primary site (data not shown). However, multiple pulmonary macrometastases were detected in both groups. The frequency of animals with lung metastases was 50% (4 of 8) for the control vehicle group and 100% (9 of 9) for the ZOL weekly treated group (Fig. 4C). In addition, the size of lung metastases was significantly greater in the ZOL-treated group, with tumor area occupying 7% of the total lung area compared with only 2% in the control vehicle group (Fig. 4D).

To determine whether the observed increase in pulmonary metastases was a general phenomenon, or peculiar to the K-HOS cell line, we extended our studies using a second OS cell line (KRIB), described previously by Berlin et al. (26) as a highly metastatic line when transplanted intratibially. As observed with K-HOS cells, treatment with ZOL *in vitro* decreased KRIB cell proliferation in a dose-dependent manner, which was concomitant with a dose-dependent increase in caspase-3 activity (Fig. 5A). DAPI staining of nuclei confirmed induction of apoptosis with ZOL treatment (Fig. 5B). ZOL administration s.c. to KRIB tumor-bearing mice, once only at the clinically relevant dose of 100 μg/kg, inhibited both the osteolytic and osteoblastic components of KRIB lesions, as assessed qualitatively by three-dimensional μCT (Fig. 5C). However, as we observed with K-HOS cells, ZOL was without effect on tumor burden at the primary site of the tibia (Fig. 5D). Unlike K-HOS cells, treatment neither reduced nor increased significantly pulmonary metastasis formation in this model (Fig. 5D), suggesting that different OSs may respond differently to ZOL treatment *in vivo*.

Discussion

In seeking to understand the molecular mechanisms by which ZOL is cytotoxic in OS cells, we have shown that the ZOL-mediated induction of OS cell apoptosis was due to the inhibition of protein prenylation and this was concomitant with an increase in caspase-3 activity. However, although caspase inhibition blocked the ZOL-induced activation of caspases, it did not prevent ZOL-induced apoptosis. These results are consistent with our previously published data on the *in vitro* cytotoxic activity of ZOL in a panel of human OS cell lines, in which we provided evidence that the induction of cell death of human OS cells by ZOL resembled "anoikis," a special mode of apoptosis that occurs when adherent cells detach or lose particular attachment contacts with the extracellular matrix that confer survival signals to the cells (17).

OSs have a variable bone-forming ability but are destructive by virtue of their ability to expand in bone by inducing osteoclast-mediated bone resorption. The effect of BPs on OS cells

Table 1. Bone morphometric parameters of tumor-injected and contralateral non–tumor-injected tibiae of vehicle-treated animals and the effect of single and weekly treatment with ZOL

Parameters	Vehicle control		ZOL × 1			ZOL weekly		
	Mean	SE	Mean	SE	*P*	Mean	SE	*P*
A. Tumor-injected tibiae								
BV (mm^3)	0.60	0.34	1.27	0.36	<0.01	1.51	0.2	<0.001
B.S. (mm^2)	81	49	151	42	<0.01	176	27	<0.01
i.S. (mm^2)	2.9	1.8	5.4	1.2	<0.01	5.6	1.4	<0.01
Tb.Sp. (mm)	0.18	0.06	0.12	0.04	<0.02	0.12	0.04	<0.03
Tb.N. (1/mm)	3.45	1.66	7.17	1.37	<0.001	7.70	1.0	<0.001
Tb.Th. (mm)	0.04	0.00	0.04	0.00	0.2	0.04	0.0	0.40
Tb.Pf. (1/mm)	6.70	23	−39	19	<0.01	43	11	<0.001
SMI	1.96	0.5	0.7	0.38	<0.001	0.6	0.36	<0.001
B. Contralateral non–tumor injected tibiae								
BV (mm^3)	0.43	0.15	1.31	0.38	<0.001	1.76	0.15	<0.001
B.S. (mm^2)	56	15.9	156	34.5	<0.001	158	16.7	<0.001
i.S. (mm^2)	3.45	1.06	6.38	1.59	<0.001	8.1	0.43	<0.001
Tb.Sp. (mm)	0.23	0.00	0.12	0.03	<0.001	0.15	0.04	<0.01
Tb.N. (1/mm)	4.34	0.90	6.76	1.22	<0.001	9.64	0.6	<0.001
Tb.Th. (mm)	0.04	0.00	0.04	0.00	0.12	0.04	0.00	<0.001
Tb.Pf. (1/mm)	−4.41	15.2	−21.3	12.1	<0.05	−70.30	6.77	<0.001
SMI	1.57	0.3	1.22	0.38	<0.04	−0.92	0.26	<0.001

NOTE: A. Bone morphometric parameters of tumor-injected tibiae of vehicle-treated animals and the effect of single and weekly treatment with ZOL. B. Bone morphometric parameters of contralateral non–tumor-injected tibiae of vehicle-treated animals and the effect of single and weekly treatment with ZOL. Trabecular bone volume, bone surface, intersection surface, trabecular space, trabecular number, trabecular thickness, trabecular pattern factor, and structure model index were measured by three-dimensional analysis of μCT images of trabecular bone only. Results are expressed as mean ± SE. Significance of results is with respect to untreated animals obtained using Student's *t* test.
Abbreviations: BV, bone volume; B.S., bone surface; i.S., intersection surface; Tb.Sp., trabecular space; Tb.N., trabecular number; Tb.Th., trabecular thickness; Tb.Pf., trabecular pattern factor; SMI, structure model index.

has not been extensively studied, although studies with alendronate and pamidronate reportedly showed proapoptotic effects on canine (18) and human (36, 37) OS cells *in vitro*. Two recent studies have reported on the effect of ZOL in animal models of mouse and rat OS. For example, Ory et al. (38) used mouse OS cells administered i.v. to show that ZOL treatment suppressed lung metastases and prolonged the overall survival of OS-bearing mice. Heymann and coworkers (30) also showed that ZOL completely prevented lung metastases and caused reduction in osteolytic lesions in a rat model, in which intact rat OS tissue was implanted s.c. and in contact with the tibial bone surface. OS originates in the bone so that the clinical relevance of animal models of OS with ectopic tumor implantation, such as i.v. injections or s.c. implantation, is not clear. Unlike these studies, our experimental model, in which OS cells are transplanted directly into the bone marrow cavity, more closely simulates the normal progression of OS and allows for the direct evaluation of ZOL treatment of OS lesions normally seen in cancer patients. Here, we show that ZOL is able to inhibit the development and progression of not only osteolytic but also the osteoblastic component of primary OS lesions. New bone formation, the so-called "sunburst spiculation," was seen in

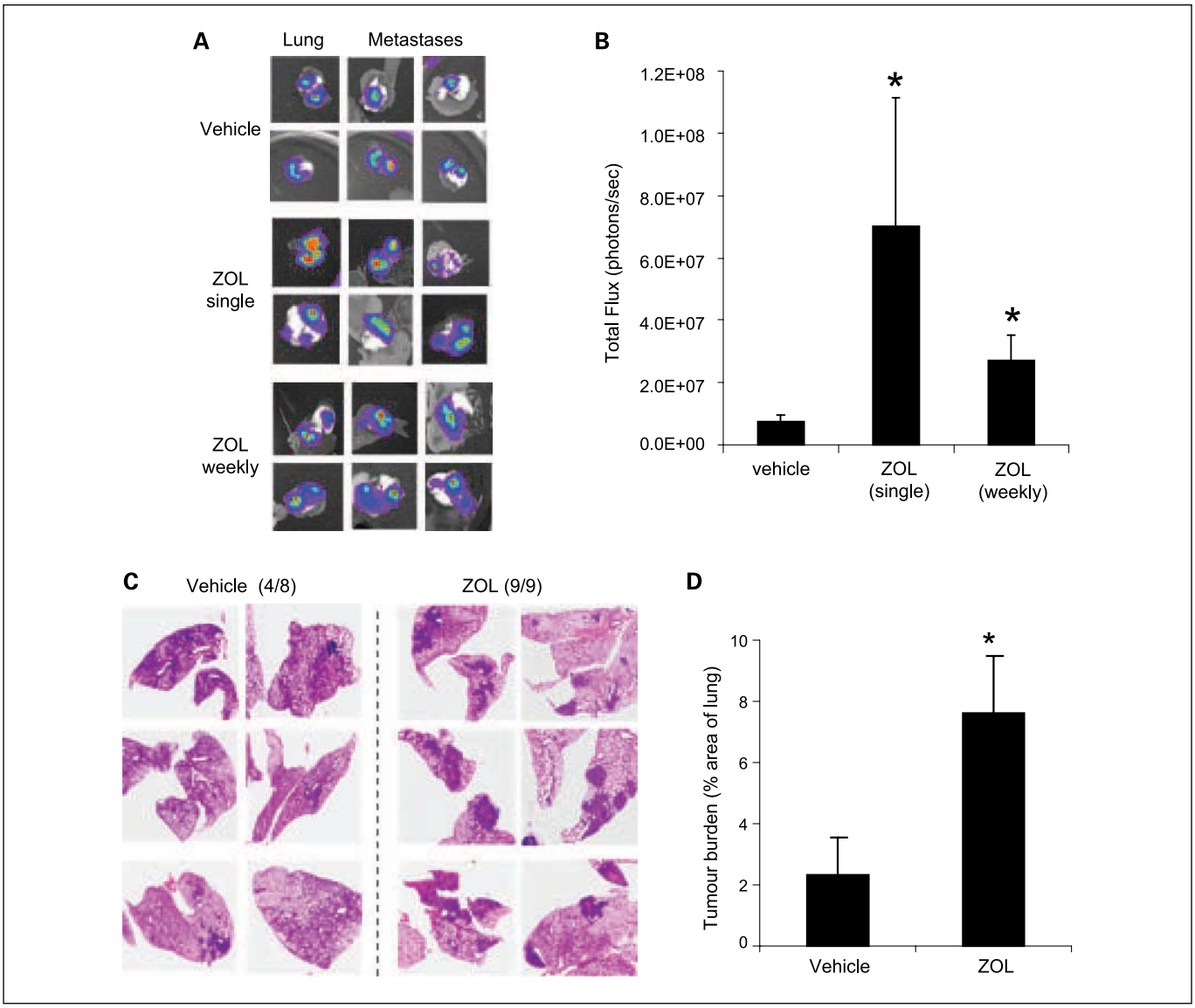

Fig. 4. Effects of ZOL treatment on pulmonary metastases. *A,* on sacrifice, the lungs were removed for BLI and quantification of tumor burden. Photos depict the signal emitted from individual lungs in each group of mice. *B,* the graph represents BLI measurements, which are expressed as the sum of integrated photon counts per second. Columns, mean; bars, SE. *, $P < 0.01$. *C,* 20 animals were inoculated with untagged parental K-HOS cells and animals were then assigned randomly into two groups: (*left*) the control untreated group and (*right*) the ZOL weekly treated group (100 μg/kg dose once weekly). Tibial tumor area was calculated from representative histologic sections and expressed as an average tumor area per group (mm^2). Tibial tumor volume (mm^3) was also measured using μCT software, as described in Materials and Methods. Despite the protective effects of ZOL on OS-induced bone destruction, ZOL had no effect on tibial tumor burden. Photographs are representative of H&E-stained sections of mouse lungs at 35 d after inoculation with K-HOS cells from vehicle- or ZOL-treated animals. Histologic sections of the lungs were photographed and used to measure tumor area and total lung area. *D,* graph represents the tumor burden in the lung expressed as percentage of total lung. Data shown in each case are an average from a representative section of each animal. Columns, mean; bars, SE. *, $P < 0.05$.

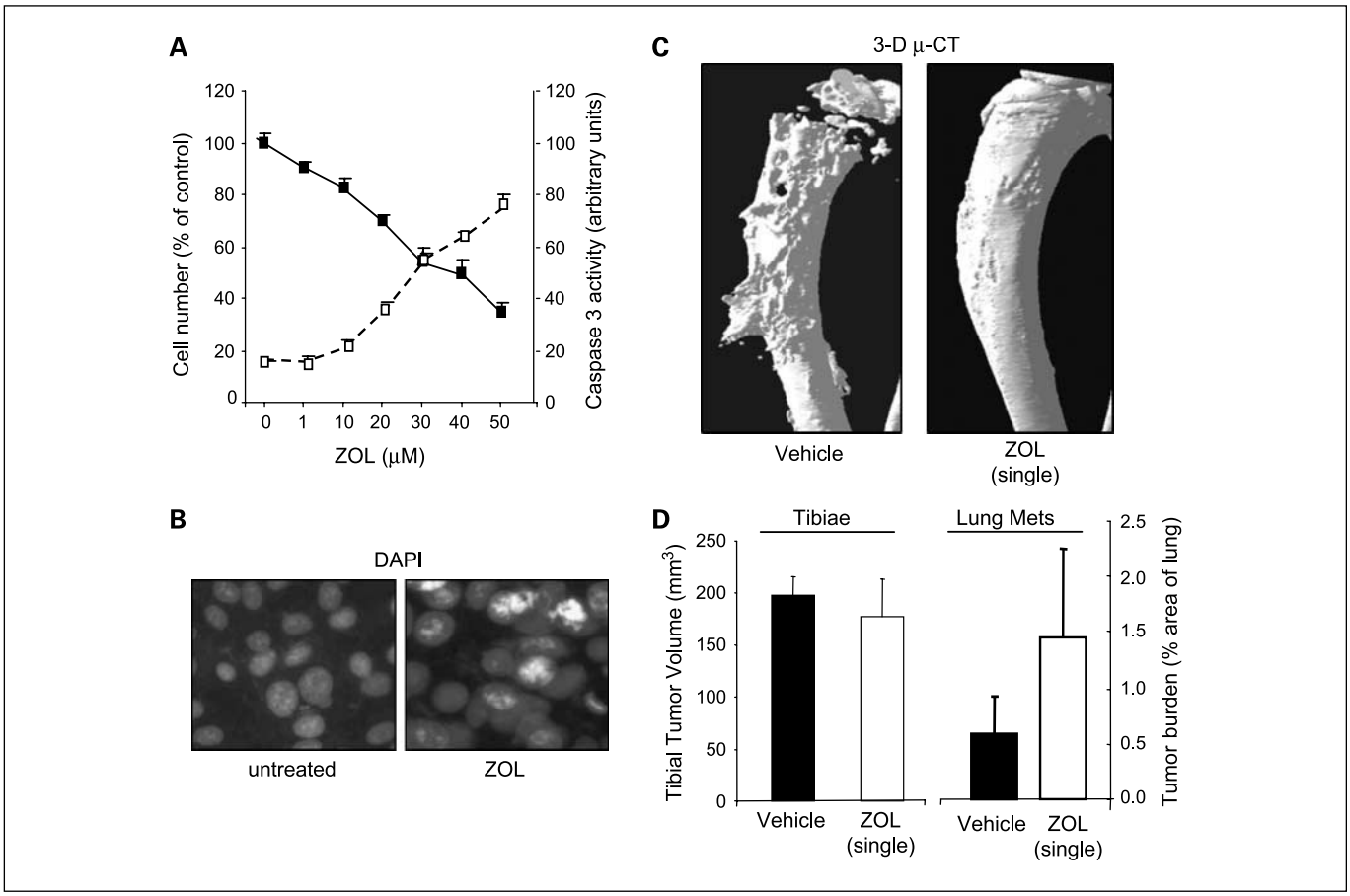

Fig. 5. Effects of ZOL on KRIB cells. *A,* KRIB cells were incubated for 72 h in medium containing increasing concentrations of ZOL (0-50 μmol/L) and cell number as a percentage of control untreated cells was determined (*solid line*). Cell lysates were used to determine caspase-3–like activity using the caspase-3–specific fluorogenic substrate, zDEVD-AFC, as described previously (*dotted line*; ref. 17). The data show a dose-dependent decrease in cell survival concomitant with a dose-dependent increase in caspase-3 activity. *B,* KRIB cells were seeded on chamber slides at 5×10^4 per chamber and were treated for 72 h with ZOL at 25 μmol/L. Cells were fixed with methanol, incubated with DAPI, and visualized by fluorescence microscopy. *C,* representative three-dimensional reconstructed μCT images (5 μm resolution) of KRIB bearing tibiae from vehicle-treated and ZOL (100 μg/kg)–treated mice showing protection from OS-induced bone destruction. *D,* tibial tumor volume (mm^3) was measured using μCT software, as described in Materials and Methods. Histologic sections of the lungs were photographed and used to measure tumor area and total lung area. Graph represents the tumor burden in the lung expressed as percentage of total lung. Data shown in each case are an average from a representative section of each animal. Columns, mean; bars, SE.

mice with xenografts after the tumor had breached the cortical bone. This is a distinctive feature of OS and is observed radiographically in ~40% of OS (39). The type of reactive new bone as shown in this study did not take place within the soft tissue of the tumor mass but was an extension of, and in contact with, the periosteum and bone cortex. Although breaching bone integrity (e.g., by drilling) can result in ectopic bone formation, we have not seen such periosteal reaction when highly osteolytic breast cancer (MDA-MB-231; ref. 40) or multiple myeloma (RPMI-8226; ref. 41) tumors breach the cortex after intratibial injection. This indicates that this effect is not the result of periosteal contact by the tumors per se but is likely to be caused by factors produced specifically by OS cells acting on osteoblast precursors within the periosteum, leading to osteogenesis.

Despite the protective effects of ZOL on OS-induced bone destruction, ZOL treatment had no effect on tumor burden at the primary site, with either the weekly ZOL dosing regimen or the clinically compatible single dose. More importantly, ZOL failed to reduce lung metastases of KRIB cells and actually promoted lung metastases of K-HOS cells. In contrast to our observations, Dass and Choong (42) have recently shown, in a similar mouse model implanted with SaOS-2 cells, that ZOL administration twice weekly at 120 μg/kg resulted in primary tumor growth inhibition, reduction in lung metastases, and dramatic decrease in osteolysis. The reasons for these different observations are not clear but may relate to cell type and, in particular, the dose of ZOL administered, which in this case was ~8-fold higher than the clinically compatible dose used in our study.

It remains unclear as to how ZOL might promote pulmonary metastases of K-HOS cells in this model. The tumor-bone microenvironment is a complex system influenced by many factors and cell types. We have shown that ZOL treatment results in increased amounts of bone at the tumor site and this is likely to alter the spatial relationship and interaction of tumor cells with the bone stroma. One could speculate that the ZOL-mediated increase in trabecular density and spatial constraints could "force" cancer cells to escape the marrow cavity, thus increasing metastatic spread. In an earlier study, we showed that ZOL treatment increased cell detachment from the substratum and

provided evidence that the induction of cell death of human OS cells by ZOL resembled anoikis, a special mode of apoptosis that occurs when adherent cells detach or lose particular attachment contacts with the extracellular matrix (17). It is possible that the same may occur *in vivo* and that cancer cells exposed to ZOL may gain metastatic potential as they lose attachment. Many studies (14–16, 18, 43–46), including our own (17), have provided *in vitro* data to suggest that ZOL has a direct effect on tumor cells, as it inhibited tumor cell proliferation and induced apoptosis. However, whether cancer cells are exposed to similar levels of ZOL *in vivo* is a contentious issue. In contrast to some previous reports, the present study showed that ZOL did not decrease tumor burden at the primary site, suggesting that the protective effects of ZOL on bone were not mediated by a direct effect on tumor cells themselves but were the result of inhibition of bone resorption.

In conclusion, our data show that clinically relevant doses of ZOL, while protecting the bone from OS-induced bone destruction, do not inhibit primary tumor growth or reduce lung metastases but in some cases can promote lung metastases. Caution is therefore required if and when the clinical application of the BP class of antiresorptives is considered in OS.

Disclosure of Potential Conflicts of Interest

No potential conflicts of interest were disclosed.

Acknowledgments

We thank Dr. Jonathan Green (Novartis, Basel, Switzerland) for helpful discussions, Dr. Peter Self (Adelaide Microscopy Centre) for his technical assistance in μCT analysis, and Prof. Peter Choong for his assistance with the intratibial injections.

References

1. Campanacci M. Bone and soft tissue tumors. 2nd ed Padova: Piccin Nuova Libraria; 1999.
2. Pringle JAS. Bone-forming neoplasms arising within bone. In: Helliwell TR, editor. Pathology of bone and joint neoplasms. Philadelphia: Saunders; 1999.
3. Link MP, Goorin AM, Horowitz M, et al. Adjuvant chemotherapy of high-grade osteosarcoma of the extremity. Updated results of the Multi-Institutional Osteosarcoma Study. Clin Orthop Relat Res 1991;8–14.
4. Saeter G, Alvegard TA, Elommaa I, et al. Chemotherapy for osteosarcoma and Ewing's sarcoma. Acta Orthop Scand Suppl 1997;273:120–5.
5. Chan HS, Grogan TM, Haddad G, DeBoer G, Ling V. P-glycoprotein expression: critical determinant in the response to osteosarcoma chemotherapy. J Natl Cancer Inst 1997;89:1706–15.
6. Mundy GR. Metastasis to bone: causes, consequences and therapeutic opportunities. Nat Rev Cancer 2002;2:584–93.
7. Goltzman D. Osteolysis and cancer. J Clin Invest 2001;107:1219–20.
8. Taube T, Elomaa I, Blomqvist C, Beneton MN, Kanis JA. Histomorphometric evidence for osteoclast-mediated bone resorption in metastatic breast cancer. Bone 1994;15:161–6.
9. Chirgwin JM, Guise TA. Molecular mechanisms of tumor-bone interactions in osteolytic metastases. Crit Rev Eukaryot Gene Expr 2000;10:159–78.
10. Goltzman D. Mechanisms of the development of osteoblastic metastases. Cancer 1997;80:1581–7.
11. Goltzman D, Karaplis AC, Kremer R, Rabbani SA. Molecular basis of the spectrum of skeletal complications of neoplasia. Cancer 2000;88:2903–8.
12. Body JJ. Current and future directions in medical therapy: hypercalcemia. Cancer Cell 2000;88:3054–8.
13. Zhang FL, Casey PJ. Protein prenylation: molecular mechanisms and functional consequences. Annu Rev Biochem 1996;65:241–69.
14. Kimura S, Kuroda J, Segawa H, et al. Antiproliferative efficacy of the third-generation bisphosphonate, zoledronic acid, combined with other anticancer drugs in leukemic cell lines. Int J Hematol 2004;79:37–43.
15. Senaratne SG, Colston KW. Direct effects of bisphosphonates on breast cancer cells. Breast Cancer Res 2002;4:18–23.
16. Lee MV, Fong EM, Singer FR, Guenette RS. Bisphosphonate treatment inhibits the growth of prostate cancer cells. Cancer Res 2001;61:2602–8.
17. Evdokiou A, Labrinidis A, Bouralexis S, Hay S, Findlay DM. Induction of cell death of human osteogenic sarcoma cells by zoledronic acid resembles anoikis. Bone 2003;33:216–28.
18. Farese JP, Ashton J, Milner R, et al. The effect of the bisphosphonate alendronate on viability of canine osteosarcoma cells *in vitro*. In Vitro Cell Dev Biol Anim 2004;40:113–7.
19. Green JR. Bisphosphonates: preclinical review. Oncologist 2004;9:3–13.
20. Peyruchaud O, Winding B, Pecheur I, Serre CM, Delmas P, Clezardin P. Early detection of bone metastases in a murine model using fluorescent human breast cancer cells: application to the use of the bisphosphonate zoledronic acid in the treatment of osteolytic lesions. J Bone Miner Res 2001;16:2027–34.
21. Daubine F, Le Gall C, Gasser J, Green J, Clezardin P. Antitumor effects of clinical dosing regimens of bisphosphonates in experimental breast cancer bone metastasis. J Natl Cancer Inst 2007;99:322–30.
22. Corey E, Brown LG, Quinn JE, et al. Zoledronic acid exhibits inhibitory effects on osteoblastic and osteolytic metastases of prostate cancer. Clin Cancer Res 2003;9:295–306.
23. Lee YP, Schwarz EM, Davies M, et al. Use of zoledronate to treat osteoblastic versus osteolytic lesions in a severe-combined-immunodeficient mouse model. Cancer Res 2002;62:5564–70.
24. Body JJ. Rationale for the use of bisphosphonates in osteoblastic and osteolytic bone lesions. Breast Cancer Res 2003;12:S37–44.
25. Ali SM, Esteva FJ, Hortobagyi G, et al. Safety and efficacy of bisphosphonates beyond 24 months in cancer patients. J Clin Oncol 2001;19:3434–7.
26. Berlin O, Samid D, Donthineni-Rao R, Akeson W, Amiel D, Woods VL. Development of a novel spontaneous metastasis model of human osteosarcoma transplanted orthotopically into bone of athymic mice. Cancer Res 1993;53:4890–5.
27. Ponomarev V, Doubrovin M, Serganova I, et al. A novel triple-modality reporter gene for whole-body fluorescent, bioluminescent, and nuclear noninvasive imaging. Eur J Nucl Med Mol Imaging 2004;31:740–51.
28. Zannettino AC, Rayner JR, Ashman LK, Gonda TJ, Simmons PJ. A powerful new technique for isolating genes encoding cell surface antigens using retroviral expression cloning. J Immunol 1996;156:611–20.
29. Rhim JS, Cho HY, Huebner RJ, Gilden RV. Characterization of Kirsten sarcoma virus transformation of human cells and isolation of nonproducer human cells. Bibl Haematol 1975;84–7.
30. Heymann D, Ory B, Blanchard F, et al. Enhanced tumor regression and tissue repair when zoledronic acid is combined with ifosfamide in rat osteosarcoma. Bone 2005;37:74–86.
31. Lamoureux F, Ory B, Battaglia S, et al. Relevance of a new rat model of osteoblastic metastases from prostate carcinoma for preclinical studies using zoledronic acid. Int J Cancer 2008;122:751–60.
32. Miller S, Jee W. Ethane-1-hydroxy-1, 1-diphoshphonate (EHDP). Effects on growth and modeling of the rat tibia. Calcif Tissue Res 1975;18:215–31.
33. Rowe D. Bone remodeling and a fluorinated bisphosphonate. Bone 1985;6:433–7.
34. Schenk R, Merz W, Muhlbauer R, Russell R, Fleisch H. Effect of ethane-1-hydroxyl-1,1-diphoshphonate (EHDP) and dichloromethylene diphosphonate (Cl_2MDP) on the calcification and resorption of cartilage and bone in the tibial epiphysis and metaphysis of rats. Calcif Tissue Res 1973;11:196–214.
35. Shinoda H, Adamek G, Felix R, Fleisch H, Schenk R, Hagen P. Structure-activity relationships of various bisphosphonates. Calcif Tissue Res 1983;35:87–99.
36. Cheng YY, Hueng L, Lee KM, Li K, Kumta SM. Alendronate regulates cell invasion and MMP-2 secretion in human osteosarcoma cell lines. Pediatr Blood Cancer 2004;42:410–5.
37. Sonnemann J, Eckervogt V, Truckenbrod B, Boos J, Winkelmann W, van Valen F. The bisphosphonate pamidronate is a potent inhibitor of human osteosarcoma cell growth *in vitro*. Anticancer Drugs 2001;12:459–65.
38. Ory B, Heymann M, Kamijo A, Gouin F, Heymann D, Redini F. Zoledronic acid suppresses lung metastases and prolongs overall survival of osteosarcoma-bearing mice. Cancer 2005;104:2522–9.
39. Wilner D. Radiology of bone tumours and allied disorders. 1982;3:1897–2095.
40. Thai le M, Labrinidis A, Hay S, et al. Apo2l/tumor necrosis factor-related apoptosis-inducing ligand prevents breast cancer-induced bone destruction in a mouse model. Cancer Res 2006;66:5363–70.

41. Labrinidis A, Diamond P, Martin S, et al. Apo2L/TRAIL inhibits tumour growth and bone destruction in a murine model of multiple myeloma. Clin Cancer Res 2009;15:1998–2009.

42. Dass CR, Choong PF. Zoledronic acid inhibits osteosarcoma growth in an orthotopic model. Mol Cancer Ther 2007;6:3263–70.

43. Sonnemann J, Eckervogt V, Truckenbrod B, Boos J, Winkelmann W, van Valen F. The bisphosphonate pamidronate is a potent inhibitor of Ewing's sarcoma cell growth *in vitro*. Anticancer Drugs 2003;14:767–71.

44. Riebeling C, Forsea AM, Raisova M, Orfanos CE, Geilen CC. The bisphosphonate pamidronate induces apoptosis in human melanoma cells *in vitro*. Br J Cancer 2002; 87:366–71.

45. Sawada K, Morishige K, Tahara M, et al. Alendronate inhibits lysophosphatidic acid-induced migration of human ovarian cancer cells by attenuating the activation of rho. Cancer Res 2002;62:6015–20.

46. Tassone P, Tagliaferri P, Viscomi C, et al. Zoledronic acid induces antiproliferative and apoptotic effects in human pancreatic cancer cells *in vitro*. Br J Cancer 2003;88: 1971–8.

Clinical Cancer Research

Zoledronic Acid Inhibits Both the Osteolytic and Osteoblastic Components of Osteosarcoma Lesions in a Mouse Model

Agatha Labrinidis, Shelley Hay, Vasilios Liapis, et al.

Clin Cancer Res 2009;15:3451-3461.